RD42 Internal Note-11
Version: September 26, 1997

Neutron Irradiation Study of CVD Diamond Detectors for High Luminosity Experiments at the LHC

PRELIMINARY

The RD42 Collaboration

Abstract

This note reports on neutron irradiations of CVD diamond and compares with irradiated silicon diodes. In several neutron irradiation runs samples received an integrated neutron fluence above 10^{15} n/cm^2. Charge collection distance was measured and observed to stay constant after irradiation with only thermal neutrons up to 2.7×10^{15} n/cm^2. After irradiation with fast neutrons (1 MeV) charge collection distance remains unchanged up to 5×10^{14} n/cm^2. Leakage currents of diamond samples were in order of pA and found to decrease after irradiation. Particle induced currents on originally unirradiated samples decrease during irradiation as well and finally saturate. The particle induced current on irradiated samples correlates with the neutron flux and the induced charge in diamond is proportional to the neutron fluence. The amount of hydrogen was estimated measuring infrared absorption coefficients for C-H bond stretching. Preliminary measurements suggest a decrease of hydrogen content with n-fluence and could explain decreasing currents in diamond. Observations on charge collection and leakage current add to other particle irradiations and confirm that diamond detectors are able to work over 10 years in high luminosity experiments at the Large Hadron Collider without replacement and loss in performance.

List of participants

Experimental Realization:
- W.Dulinski
- M.Edwards
- R.Hall-Wilton, and R.J.Tapper
- D.Meier

Analysis:
- W.Dulinski
- M.Edwards
- D.Meier
- H.Kagan
- B.Stone
- M.Zoeller

Authors and Critics received from:
- D.Husson
- D.Meier
- H.Kagan
- W.Trischuk
- P.Weilhammer

1 Introduction

At present silicon strip detectors are used with great success for high precision tracking of charged particles. However the radiation resistance of silicon puts limits to its application. In a high radiation environment problems occur with increasing leakage currents and decreasing charge collection efficiency. Detectors in future collider experiments at the Large Hadron Collider, LHC, will be exposed to extremly high radiation levels. Silicon strip detectors might be usable up to 10 Mrad or 10^{14} n/cm^2 in a permanently cooled environment of $-5°$C. At a distance of 10 cm from the beam axis, detectors are expected to receive a neutron fluence of $7{\times}10^{14}$ per cm^2 during 10 years of operation at a beam luminosity of 1×10^{34} /cm^2/s. The fluence decreases with distance from the beam axis and reaches at 20 cm distance 2.2×10^{14} n/cm^2 and decade [1]. Similar orders of magnitude are expected for protons an pions. At present silicon pixel detectors are proposed in this region [2]. Another possibility is diamond, whose properties make it an ideal material for particle detectors [3]. Detector grade diamond can be grown with chemical vapor deposition, CVD, technique producing a polycristalline diamond structure. After metalization with strip or pixel electrodes it can be used for particle tracking [4]. The number of charges which can be collected from CVD diamond substates of recent growths amounts in mean 7200 e which corresponds to a charge collection distance of 200 μm [5].

It has been shown in the past that CVD diamond is resistant to purely electromagnetically interacting radiation up to a dose of 100 Mrad [3, 6]. Moreover in proton and pion irradiations of up to 2×10^{15} p/cm^2 and 1.7×10^{15} π/cm^2 no decrease in charge collection was found [7, 5]. The performance of CVD diamond detectors after neutron irradiation has to be studied as well since neutrons will be present in any experiment at the LHC and might damage the crystall lattice of a detector significantly.

1.1 Samples in Neutron Irradiation

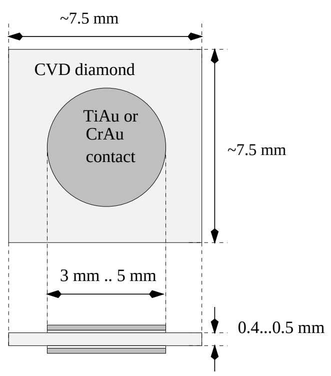

Figure 1: Geometry and size of diamond samples, top- and sideview. The diamond samples were metalized with ohmic contacts on both sides.

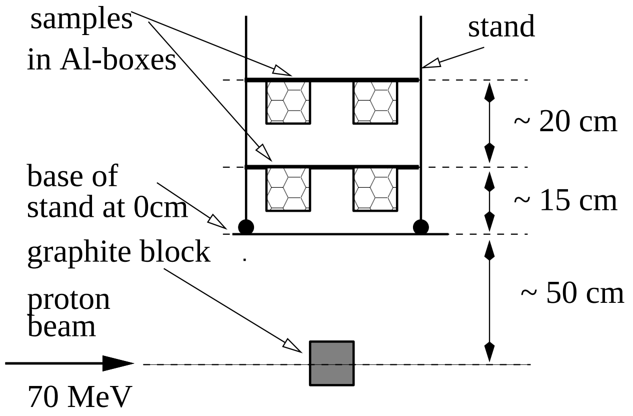

Figure 2: Sideview of the sample stand and spallation target at ISIS. The samples were mounted in different distance from the collector box in order to receive different neutron fluences.

CVD diamond wafers were grown with a size of 4” and a thickness in an order of 400 μm [8, 9]. Rectangular samples of 7.5×7.5 mm^2 were cut from these wafers and metallized on both sides with round electrodes of a diameter between 3 mm and 5 mm [Fig. 1]. The electrodes were made of CrAu or TiAu forming ohmic contacts to the diamond substrate. A set of 13 CVD diamond samples and 5 silicon diodes were chosen for irradiation [Tab. 1].

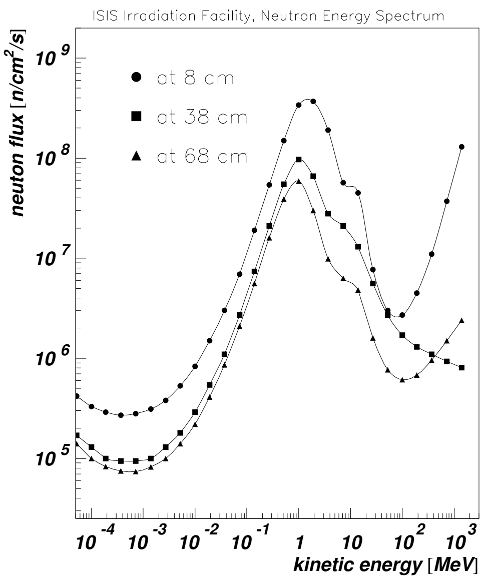

Figure 3: Kinetic energy spectrum of neutrons at ISIS taken at different heights from the graphite block [10].

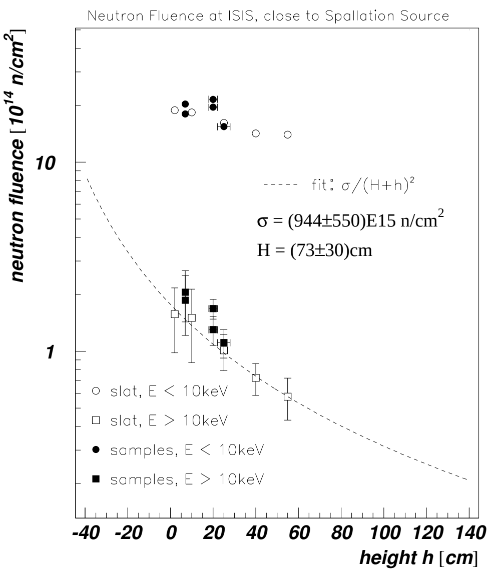

Figure 4: Neutron flux versus distance from the graphite block .

1.2 Irradiation Setup

All samples were irradiated at ISIS, a neutron source at the Rutherford Appleton Laboratory. Irradiations were done using four run periodes in 1/95, 10/95, 12/95 and 11/96. Neutrons were produced in a spallation process from a graphite block backed with copper [Fig.2]. The graphite block was mounted in a collector box along the beam pipe between the injection and extraction lines of the proton synchrotron ring. Protons at that point have an energy of 70 MeV and those which are lost by the accelerating fields interact in the graphite block producing neutrons, which escape isotropically from the graphit block. All samples were fixed in aluminum boxes and tighed to a stand in different distances from the collector box.

1.3 Dosimetry

The kinetic energy spectrum of neutrons measured on the sample stand is shown in Fig.3 [10]. The spectrum shows fast neutrons with kinetic energy above 10 keV, peaks at 1 MeV and decreases to half maximum at 10 MeV. Thermal or slow neutrons with kinetic energy below 10 keV are present as well.

The number ΔN_p of protons which are lost by the accelerating field interact in the graphite block and produce in a time interval Δt a number ΔN_n of neutrons. The proton current $e\Delta N_p/\Delta t$ is proportional to the injected proton current $I_{p,\mathrm{inj}}$ and therefore $\Delta N_n/\Delta t \propto I_{p,\mathrm{inj}}$. The neutron flux $f_n = \Delta N_n/\Delta A/\Delta t$ is given by the number of neutrons passing an area element $\Delta A = r^2 \mathrm{d}\Omega$ at distance r from the graphite block during the time Δt, where neutrons are emitted isotropically into solid angles $\Delta\Omega$. Therefore one obtains the following expression for the neutron flux

$$f_n \propto \frac{I_{p,\mathrm{inj}}}{r^2}. \tag{1}$$

Integration of flux over time gives the neutron fluence which is expected to show the same $1/r^2$-dependence. The total n-fluence accumulated by each sample was measured after irradiation from γ-activity of metal foils which were attached to aluminum boxes containing the samples. Fig. 4

shows the dose measurements as a function of the distance from the base of the stand which is about 50 cm from the spallation source. The dose values for neutrons above 10 keV can be fitted with a $1/r^2$-function and agree with Equation 1.

Tab. 1 shows all irradiated samples, their thickness, electrode type, size and neutron fluence received during an irradiation run. The highest fluence of 1.85×10^{15} n/cm^2 with fast neutrons was received by Y1 during two run periodes. The lowest fluence of 3.2×10^{14} n/cm^2 with fast neutrons was received by U6 and YE. Diamond samples Y4 and YB were exposed to thermal neutrons only whereas the other samples received fast neutrons, too. Several samples were irradiated twice or three times. The given neutron fluence is the value for a single run periode. Silicon diodes S-9 and S-10 were irradiated in 10/95, S-16, S-24 and a silicon strip detector in 11/96. All of them received a fluence in order of 5×10^{14} n/cm^2.

sample name	thickness [μm]	electrode size [mm^2]	run	measured fluence [n/cm^2] at energy < 10 keV	> 10 keV
Y1	407	12.6	1/95	$(8.94 \pm 0.15) \times 10^{15}$	$(1.29 \pm 0.14) \times 10^{15}$
			10/95	$(1.57 \pm 0.03) \times 10^{15}$	$(5.62 \pm 1.39) \times 10^{14}$
			11/96	$(1.80 \pm 0.03) \times 10^{15}$	$(2.05 \pm 0.62) \times 10^{14}$
Y2	418	15.9	1/95	$(4.33 \pm 0.09) \times 10^{15}$	$(2.90 \pm 0.35) \times 10^{14}$
			10/95	$(1.48 \pm 0.03) \times 10^{15}$	$(3.17 \pm 0.58) \times 10^{14}$
Y4	414	19.6	1/95	$(2.25 \pm 0.4) \times 10^{15}$	$(6.00 \pm 0.95) \times 10^{13}$
			10/95	4.8×10^{14}	
YB	419	15.9	10/95	4.8×10^{14}	
YE	419	19.6	10/95	$(1.48 \pm 0.03) \times 10^{15}$	$(3.17 \pm 0.58) \times 10^{14}$
YF	414	19.6	10/95	$(1.57 \pm 0.03) \times 10^{15}$	$(5.62 \pm 1.39) \times 10^{14}$
U6	436	12.6	10/95	$(1.48 \pm 0.03) \times 10^{15}$	$(3.17 \pm 0.58) \times 10^{14}$
			11/96	$(2.15 \pm 0.04) \times 10^{15}$	$(1.68 \pm 0.20) \times 10^{14}$
N1	329	19.6	12/95	$(1.98 \pm 0.04) \times 10^{15}$	$(4.02 \pm 0.73) \times 10^{14}$
			11/96	$(1.54 \pm 0.03) \times 10^{15}$	$(1.11 \pm 0.19) \times 10^{14}$
N2	333	19.6	12/95	$(1.98 \pm 0.04) \times 10^{15}$	$(4.02 \pm 0.73) \times 10^{14}$
			11/96	$(2.15 \pm 0.04) \times 10^{15}$	$(1.68 \pm 0.20) \times 10^{14}$
N3	354	12.6	12/95	$(2.01 \pm 0.04) \times 10^{15}$	$(5.45 \pm 1.79) \times 10^{14}$
			11/96	$(2.03 \pm 0.04) \times 10^{15}$	$(1.86 \pm 0.65) \times 10^{14}$
U7	433	12.6	12/95	$(2.01 \pm 0.04) \times 10^{15}$	$(5.45 \pm 1.79) \times 10^{14}$
			11/96	$(1.80 \pm 0.03) \times 10^{15}$	$(2.05 \pm 0.62) \times 10^{14}$
P3	755	7.1	11/96	$(1.95 \pm 0.03) \times 10^{15}$	$(1.30 \pm 0.23) \times 10^{14}$
P4	728	7.1	11/96	$(2.03 \pm 0.04) \times 10^{15}$	$(1.86 \pm 0.65) \times 10^{14}$
S-9	350	16.0	10/95	$(1.48 \pm 0.03) \times 10^{15}$	$(3.17 \pm 0.58) \times 10^{14}$
S-10	350	16.0	10/95	$(1.57 \pm 0.03) \times 10^{15}$	$(5.62 \pm 1.39) \times 10^{14}$
S-16	350	16.0	11/96	$(1.54 \pm 0.03) \times 10^{15}$	$(1.11 \pm 0.19) \times 10^{14}$
S-24	350	16.0	11/96	$(1.54 \pm 0.03) \times 10^{15}$	$(1.11 \pm 0.19) \times 10^{14}$
SiStrip	350		11/96	$(1.54 \pm 0.03) \times 10^{15}$	$(1.11 \pm 0.19) \times 10^{14}$

Table 1: Neutron fluences on diamond samples and silicon (S-9,10,16,24, SiStrip).

The neutron flux for neutrons above 10 keV is in order of 10^8 $n/\mathrm{cm}^s/\mathrm{s}$. For e.g. 820 h irradiation in 11/96 and a final fluence of 2×10^{14} n/cm^2 we calculate a neutron flux of 6.8×10^7 $n/\mathrm{cm}^s/\mathrm{s}$.

2 Charge Collection Properties

The charge $Q_{\rm col}$ which can be collected at the electrodes after one charged particle traversed the diamond characterizes the performance of the detector. A minimum ionizing particle *mip* deposits 245 keV in $D = 500$ μm thick diamond. The energy which is necessary to excite one *eh*-pair in diamond is 13.6 eV. One obtains the number $\langle Q_{mip,\rm gen}\rangle / D = 36$ e/μm of generated electrons or holes [11] Electron hole pairs seperate in the applied electric field and travel towards the electrodes where they induce a charge $Q_{\rm col}$. The mean measured charge $\langle Q_{\rm col}\rangle$ is related to the charge collection distance d of the diamond bulk and in an approximation one finds [11]

$$d \approx \frac{\langle Q_{\rm col}\rangle}{\langle Q_{mip,\rm gen}\rangle / D} = \frac{\langle Q_{\rm col}\rangle}{36\ e/\mu\rm m}, \tag{2}$$

which relates the charge collection distance to the collected charge at the electrodes.

2.1 Setup to Measure Charge Collection Distance

Fig. 5 shows a schematics how charge collection distance was measured. A diamond sample is mounted underneath a colimated ^{90}Sr source. ^{90}Sr is a β-source and emits electrons with an endpoint energy of 2.28 MeV. A silicon diode below the diamond triggers on electrons which

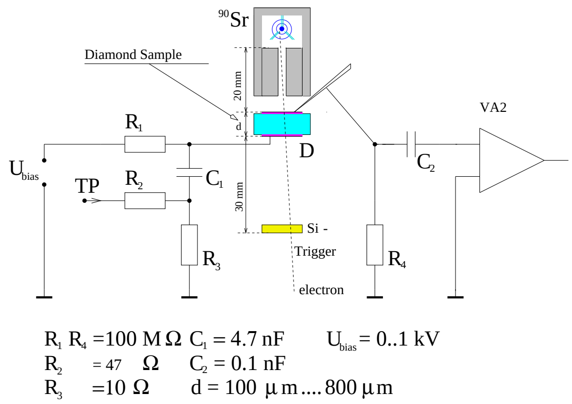

Figure 5: Setup for charge collection measurement in a diamond detector sample. The sample is illuminated by a colimated ^{90}Sr β source. A silicon diode below the diamond trigger the read-out of the charge signal in diamond.

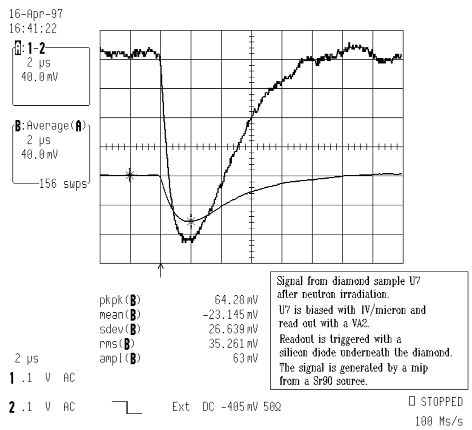

Figure 6: Signal of an event measured on diamond U7 after neutron irradiation. The signal is read out using one channel of a VA2. The shaped signal has a peaking time of 2 μs. The waveform is averaged over several events and displayed as well.

traversed the diamond. The induced charge is measured with a charge sensitive amplifier which gives the the charge collection distance [Eq.2]. The setup was calibrated in units of $e = 1.602\times10^{-19}$ C by measuring the charge signal either from a voltage pulse into a capacitor or by photo absorption from a γ-emitter in a silcion diode. Both methods give the same calibration constant with a systematic calibration error of 5%. A characteristic signal from an irradiated diamond U7 measured at an applied electric field of 1 V/μm is shown in Fig. 6. The upper waveform, trace A, shows the shaped signal from the VA2, the lower waveform is the average over several event samplings and shows about 64 mV. Using a gain of 25.5 e/mV one obtains a mean collected charge of 1630 e which corresponds to a charge collection distance of 45 μm.

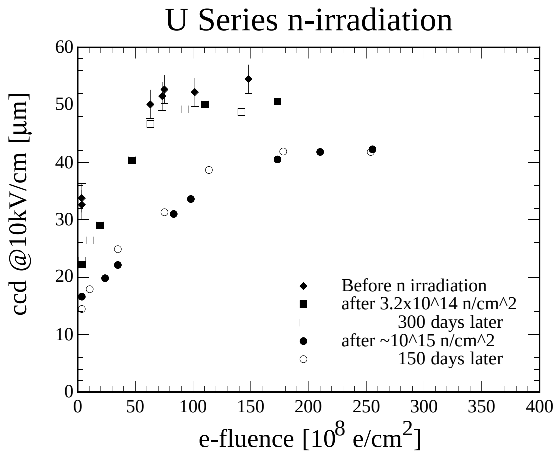

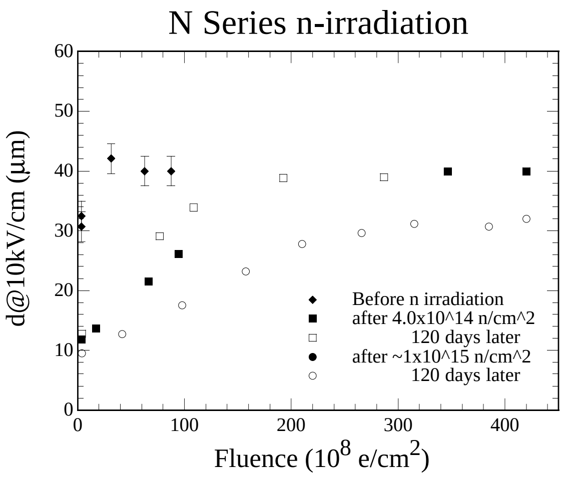

Figure 7: Charge collection distance ccd in CVD diamond samples as a function of the electron fluence before and after neutron irradiations.

2.2 Pumping with Electrons

It is known that the charge collection distance at constant voltage increases under illumination with γ or β radiation [3, 6]. On unirradiated samples an increase by a factor of 1.6 to 2.0 below 10 krad absorbed dose is observed. Above 10 krad charge collection distances stays constant. The increase at relatively low dose is called pumping. It is attributed to trap filling which then allows charge carriers to travel longer distances before being traped. A sample can be depumped by exposure to fluorescent light and charge collection distance returns to its original value. Depumping is explained by releasing filled traps. The effects of pumping and depumping are reproducible.

Fig. 7 shows the charge collection distance at 1 V/μm in samples U6 and U7 to the left and N1 and N2 to the right as a function of the fluence before and after neutron irradiations. Charge collection distance increases from a depumped value linearly with e-fluence and saturates above a certain e-fluence at its fully pumped value. After irradiation samples show a lower depumped value than before irradiation. Looking only at samples which received a n-fluence below 4.0×10^{14} n/cm^2 shows that their pump-up-curve saturates at the same value than before n-irradiation, but it requires a higher e-fluence on irradiated samples to reach saturation. Samples which received $\approx 1 \times 10^{15}$ n/cm^2 saturate 15% below the pumped value from before irradiation.

2.3 Irradiation with Thermal or Slow Neutrons

Two samples YB and Y4 were irradiated with thermal or slow neutrons only. Both samples were placed outside of the concrete shielding, 7 m from the spallation source. The fluence of slow neutrons of 2.25×10^{15} n/cm^2 in 1/95 and 4.8×10^{14} n/cm^2 in 10/95 was obtained with a negligible fraction of fast neutrons.
The charge collection distance on the pumped sample YB as a function of the applied electric field is shown in Fig. 8. Before irradiation a charge collection distance of 50 μm at 1 V/μm was observed. After irradiation with 4.8×10^{14} n/cm^2 charge collection distance is higher at an electric field below 1 V/μm and has the same value above 1 V/μm compared to the non irradiated state.
Also on sample Y4 which received thermal neutrons up to 2.7×10^{15} n/cm^2 and fast neutrons of 6.0×10^{13} n/cm^2 charge collection is the same as before irradiation.
We observe no decrease in charge collection distance due to only thermal neutrons up to 2.7×10^{15} n/cm^2 is observed.

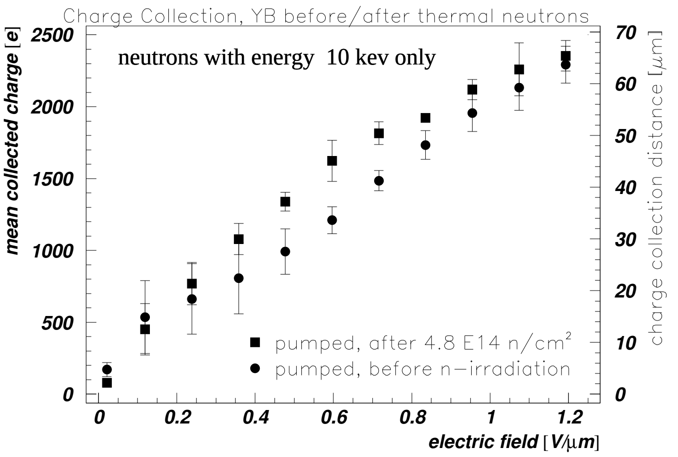

Figure 8: Charge collection distance on sample YB as a function of the applied electric field before and after irradiation with thermal neutrons.

2.4 Fast Neutrons up to a Fluence of 5×10^{14} n/cm^2

Fig. 9 shows the charge collection distance on sample U6 in the pumped state before and after irradiation 10/95 as a function of the applied electric field. Before irradiation a charge collection distance of 50 μm was measured at 1 V/μm. After irradiation with fast neutrons up to 3.2×10^{14} n/cm^2 in 10/95 charge collection distance reaches the same value as before irradiation. The measurement on U6 after its second irradiation in 11/96, when it received an additional

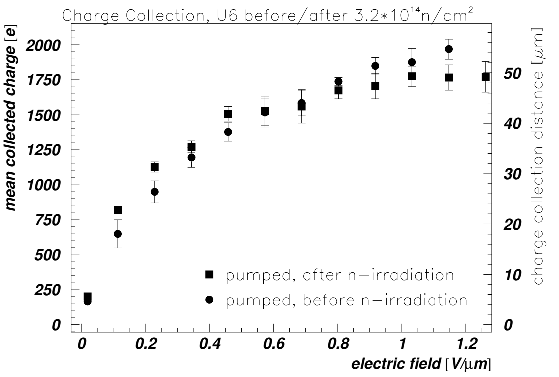

Figure 9: Charge collection distance on sample U6 as a function of the applied electric field before and after n-irradiation 10/95.

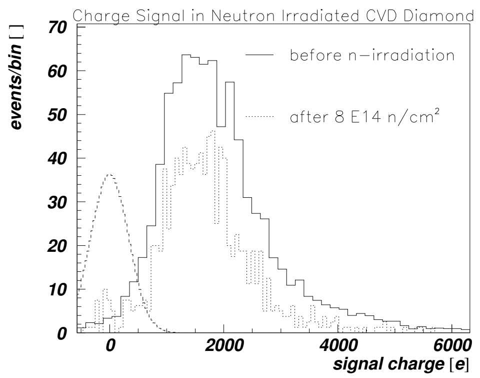

Figure 10: Signal distribution on sample U7 before and after two n-irradiations, measured after 11/96. The sample acquired a fluence of $\approx 1 \times 10^{15}$ n/cm^2. The mean signal decreases by 10%.

fluence of 1.7×10^{14} shows the same value 50 μm as before irradiation [Tab. 2]. Sample Y2, YE were irradiated with fluences below 5×10^{14} n/cm^2. Neither of them showed a decreasing charge collection distance.

2.5 Fast Neutrons above a Fluence of 5×10^{14} n/cm^2

The charge signal distribution on the pumped sample U7 before any n-irradiation and after irradiation 11/96 is shown in Fig. 10. Sample U7 accumulated after 11/96 a total fluence of 7.5×10^{14} n/cm^2. The mean value on the unirradiated sample is at 1900 e ($d = 53$ μm) and decreases after both n-irradiations by $\approx$10% to 1700 e ($d = 47$ μm). Sample Y1 received the highest fluence

sample name	fluence 11/96 > 10 keV, [n/cm2]	$d_{\text{before}11/96}$		$d_{\text{after}11/96}$	
		depumped	pumped	depumped	pumped
Y1	$(2.05 \pm 0.62) \times 10^{14}$	10	35	11	29
U6	$(1.68 \pm 0.20) \times 10^{14}$	33	50	19	50
U7	$(2.05 \pm 0.62) \times 10^{14}$	21	42	17	47
N1	$(1.11 \pm 0.19) \times 10^{14}$	17	46	13	39
N2	$(1.68 \pm 0.20) \times 10^{14}$	10	45	15	39
N3	$(1.86 \pm 0.65) \times 10^{14}$	10	32	5	19
DB43-P3	$(1.30 \pm 0.23) \times 10^{14}$	-	87	66	96
DB43-P4	$(1.86 \pm 0.65) \times 10^{14}$	-	86	33	55

Table 2: Charge collection distance measured on diamond samples before and after n-irradiation 11/96.

sample name	pumped *ccd* [μm] after each irradiation			
	0.	1.	2.	3.
Y1	≈42	40	35	29
U6	52	51	50	
U7	55	42	47	
N1	45	46	39	
N2	44	45	39	
N3	36	32	19	
DB43-P3	87	96		
DB43-P4	86	55		

Table 3: Charge collection distance of the pumped state measured on diamond samples after a certain irradiation run.

in three irradiation runs. The charge collection distance of the pumped state decreased after at 1.85×10^{15} n/cm^2 by $\approx$ 15%. After receiving an additional fluence of 2.05×10^{14} n/cm^2 giving a total fluence of 2.1×10^{15} n/cm^2 charge collection distance decreased by 30% compared to its unirradiated value. Sample N3 accumulated after its second irradiation a total fluence of 7.3×10^{14} n/cm^2. Its pumped charge collection distance decreased by about 50%. Sample N3 shows the highest decrease in charge collection distance observed on a sample after n-irradiation.

2.6 Irradiation of DeBeers Samples

Two samples from DeBeers [9] were irradiated with neutrons for the first time in 11/96. Both samples had TiAu contacts in contrary to all other samples which had CrAu contacts. The charge signal distribution on both samples before and after irradiation is shown in Fig. 11. The measurement on these samples were difficult since their contacts had a small area of 7 mm^2 and a significant fraction of events triggered signal readout although particles did not pass the contact area. This contributes to events in the pedestal. Modification of the colimator improved the situation and less events appear in the pedestal of histogramms which were measured after 11/96. The mean value of the charge signal could be calculated by excluding the pedestal events.

Sample P3 which received a fluence of 1.3×10^{14} n/cm^2 shows no decrease in charge collection distance. Sample P4 received a higher fluence of 1.9×10^{14} n/cm^2. Its charge collection distance decreases by 35%. The decrease in charge collection on P4 sets in at a relatively low fluence and is not seen on samples from Norton. The unirradiated samples from Norton show charge collection distance between 50 μm and 60 μm whereas both unirradiated DeBeers samples show a higher charge collection above 80 μm. The measurement on P4 have to be completed with further measurements and DeBeers samples with higher charge collection distance will be irradiated in the future.

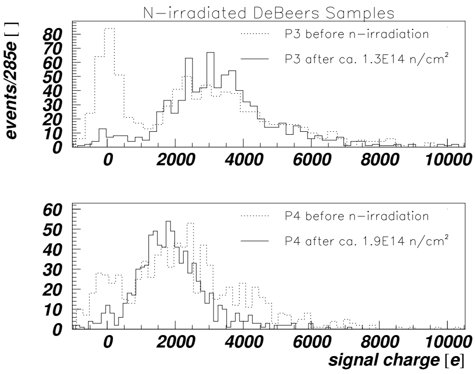

Figure 11: Charge signal distribution on samples P3 and P4 from DeBeers in the pumped state before and after neutron irradiation in 11/96.

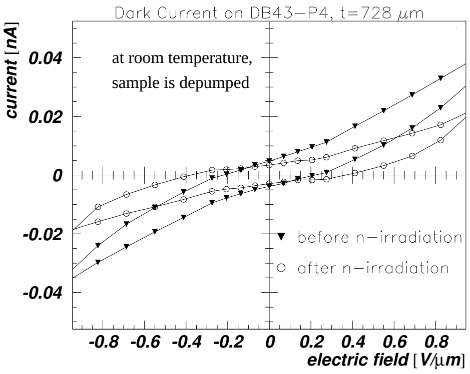

Figure 12: Dark current at roomtemperature as a function of the applied electric field on sample DB43-P4 before and after n-irradiation. The dark current is decreased after irradiation.

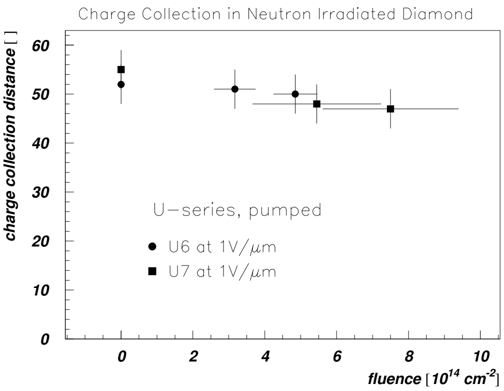

Figure 13: Charge collection distance in pumped CVD diamonds U6 and U7 as a function of the n-fluence.

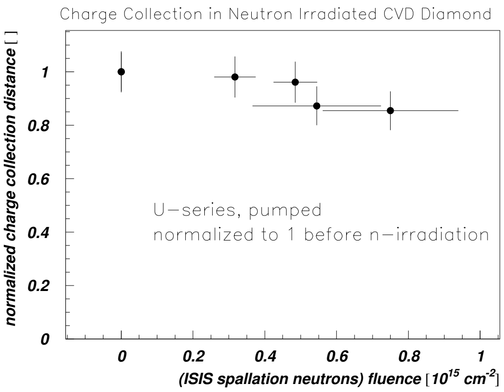

Figure 14: Charge collection distance in CVD diamond or U-series as a function of the n-fluence. The charge collection distance is normalized to its pumped value before n-irradiation.

2.7 Charge Collection versus Neutron Fluence

Fig. 13 to 18 show the charge collection distance in the pumped state as a function of neutron fluence on all samples from Norton. The samples are ordered according to their series, U-, N-, or Y-series. The U-series with U6 and U7 stays shows a slightly decreasing charge collection distance by 15% at 8×10^{14} n/cm^2. The N-series with particularly N3 drops above 5×10^{14} n/cm^2 and decreases to 50% at $\approx 8 \times 10^{14}$ n/cm^2. The Y-series suggest no decrease before $\approx 1.3 \times 10^{15}$ n/cm^2 which is based on sample Y1. Looking at YF we observe a decrease like in the N series at 5×10^{14} n/cm^2.

Fig. 19 and 20 show the absolute and normalized charge collection distances of all samples sumperimposed. Only Y1 stretches out to more than 1×10^{15} n/cm^2 without significant loss in charge collection. The other samples give strong indication that charge collection distance decreases at 5×10^{14} n/cm^2. These plot only contains data taken on Norton smaples. Both DeBeers samples P3 and P4 are not included. Further Measurements are in preparation.

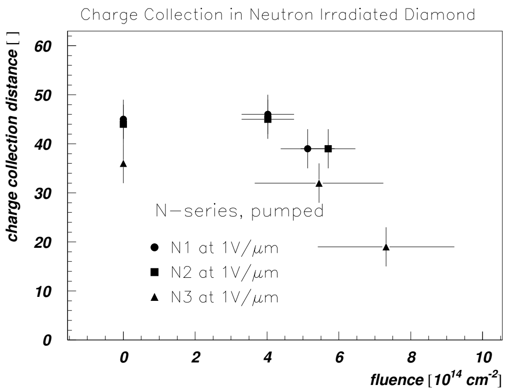

Figure 15: Charge collection distance in pumped CVD diamonds N1,N2 and N3 as a function of the n-fluence.

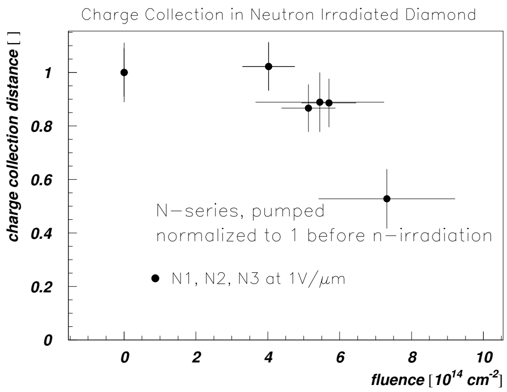

Figure 16: Charge collection distance in CVD diamonds of N-series as a function of the n-fluence. The charge collection distance is normalized to its pumped value before n-irradiation.

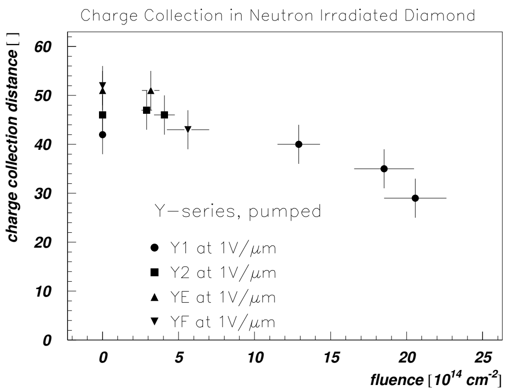

Figure 17: Charge collection distance in pumped CVD diamonds Y1, Y2, YE and YF as a function of the n-fluence.

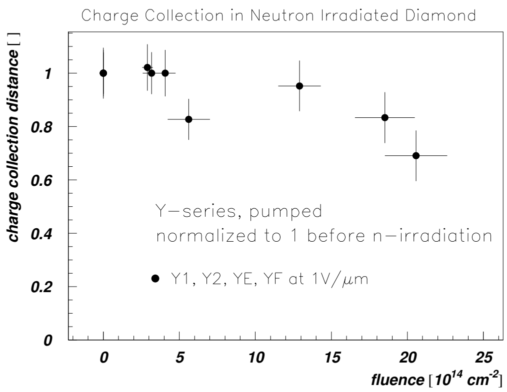

Figure 18: Charge collection distance in CVD diamonds of Y-series as a function of the n-fluence. The charge collection distance is normalized to its pumped value before n-irradiation.

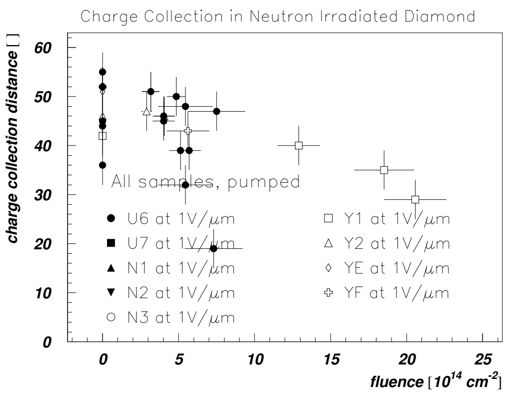

Figure 19: Charge collection distance in pumped CVD diamonds as a function of the n-fluence.

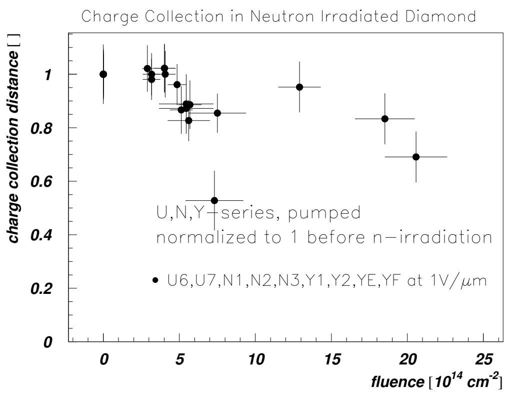

Figure 20: Charge collection distance in CVD diamonds of U,N and Y-series as a function of the n-fluence. The charge collection distance is normalized to its pumped value before n-irradiation.

3 Dark Current

The dark current density j_{dark} on diamond samples depends on the bulk conductivity σ_{bulk} and on surface properties. Surface currents should be negligible in case of an uncontaminated surface and a dark environment. The remaining bulk current is in a first approximation proportional to the applied electric field E and the dark current is given by Ohms law $j_{\text{dark}} = \sigma_{\text{bulk}} E$. The influence of fringe fields on the dark current and a non uniform field strength between both contacts are unknown and not considered. A characteristic curve of the dark current in diamond as a function of the applied electric field is shown in Fig. 12. The dark current shows hysteresis which means that the current depends on the size of the voltage step and the time between steps. This effect is explained by resistivity and capacitance introduced by the contacts. The capacitance is about 2 pF to 3 pF on samples used in the irradiation.

The conductivity for direct current was measured at 1 V/μm [Tab.4]. The dark current in diamond and therefore its conductivity depends at constant temperature on the pumping state. This effect is known on unirradiated samples and conductivity on samples in Tab.4 before irradiation increases by factor 3 to 5 after pumping. The conductivity after neutron irradiation is in general smaller by about a factor 2 for depumped values depending on the fluence. The difference in conductivity between pumped and depumped state after irradiation is significantly smaller than before neutron irradiation. This is in particular true for samples N1, N2, P3 and P4 which received a relatively low fluence or no neutrons before 11/96.

sample	σ_{before} [10^{-11} Ω^{-1}cm^{-1}] $\pm$ 10%		σ_{after} [10^{-11} Ω^{-1}cm^{-1}] $\pm$ 10%	
name	depumped	pumped	depumped	pumped
Y1	4.0	5.5	3.0	4.8
U6	5.5	14.3	3.0	4.0
U7	4.8	11.9	3.6	3.6
N1	2.7	13.3	1.2	2.3
N2	3.0	9.7	1.3	1.5
N3	-	11.1	2.8	2.8
DB43-P3	43.5	142.8	16.9	19.6
DB43-P4	62.5	250.0	33.3	38.5

Table 4: Conductivity σ before and after neutron irradiation 11/96.

4 Particle Induced Currents during Neutron Irradiation

Charged particles induce a current I_{pic} in diamond which adds to the dark current and which is given by the number of collected charges ΔQ_{col} within a time interval Δt

$$I_{\text{pic}} = \frac{\Delta Q_{\text{col}}}{\Delta t}. \tag{3}$$

Neutrons ΔN_n interact in diamond with carbon or hydrogen and produce charged particles like protons or α-particles [Sec.6]. Gamma-rays are background radiation and interact in diamond as well. Both n and γ generate a charge $\Delta Q_{n,\text{gen}}$ and $\Delta Q_{\gamma,\text{gen}}$. Using the charge collection distance d [Eq.2] one obtains

$$I_{\text{pic}} = d \cdot \frac{A}{D} \left(f_n \frac{\Delta Q_{n,\text{gen}}}{\Delta N_n} + f_\gamma \frac{\Delta Q_{\gamma,\text{gen}}}{\Delta N_\gamma} \right). \tag{4}$$

Under the assumption that the γ-flux is proportional to the n-flux one finds the induced current proportional to the neutron flux and to the charge collection distance. This equation could also be expressed in terms of cross sections since the number of generated charges per neutron or γ is proportional to the cross section.

4.1 Setup to Measure Current during Irradiation

All diamond samples were biased with a voltage of 100 V applied between both electrodes. Biasing of samples is a realistic operation condition and allows to measure induced currents during irradiation. The temperature during irradiation was stable at $(19 \pm 1)^{\circ} C$ for diamond and silicon. Fig. 21 shows the schematics for voltage biasing and current measurement on one sample. Box 1 contains the biasing voltage with a picoAmperemeter. Box 2 with the diamond sample inside was located 80 m away inside the proton hall at the irradiation zone and connected with two BNC lines to the biasing in box 1. The current through each sample was measured with accuracy of few picoAmpere during irradiation on each sample. Silicon diodes were biased with 80 V in equivalent setups but with bias resistors of 10 kΩ in order to reduce voltage drop since the expected leakage current in silicon was 10^5 times higher than in diamond.

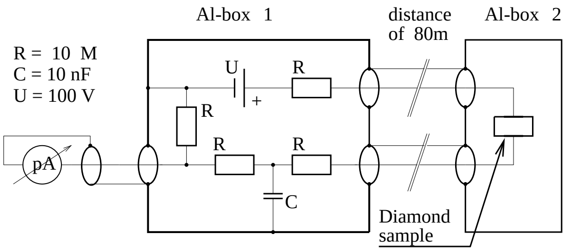

Figure 21: Circuitry for biasing diamond and silicon samples and measuring currents during n-irradiation. The current can be measured with pA accuracy over a distance of 80 m.

4.2 Current during Irradiation

A few hours before n-irradiation currents were measured on two samples U6 and YF [Fig. 22]. Between application of bias voltage and start of the irradiation currents decrease exponentially and saturate. No neutrons were present at that time. The currents saturate at 44 pA and 65 pA which indicates that the samples are either in a pumped state or that γ-backround induces charge. The contact area of U6 is 12.6 mm^2 and compared to YF with 19.6 mm^2 smaller by a factor of 0.64. The different contact area could explain the difference in both currents. The saturated current density in both samples is 3.5 pA/mm^2 and 3.3 pA/mm^2 and nearly the same.

As soon as the irradiation starts and neutrons become present currents rise to 2.0 nA and 2.7 nA [Fig. 23]. The presence of either neutrons or γ-background induces charge in the samples which lead to such an increase. During irradiation currents decrease exponentially. The exponential fit predicts a saturation current of 0.62 nA and 0.95 nA corresponding to current densities of 49.2 pA/mm^2 and 48.5 pA/mm^2. The flux of fast neutrons on both samples stays nearly constant during irradiation which indicates that the decreasing current is not due to changes in neutron flux. Although sample YF received a higher flux than U6 its current density is equal to U6. Both samples have the same charge collection distance which shows that the higher current in YF is not due to the higher flux but rather to its larger electrode. The fluence on U6 is bigger by 0.56 compared to YF [Tab.1]. Nevertheless decreases the current in both samples with the same time constant of 110 h and one concludes that the current decrease is not related to the fluence of fast neutrons.

The current on another sample U7 was measured during two irradiations 12/95 [Fig. 24] and 11/96 [Fig. 25]. The measurement was done automatically every 5 minutes and has therefore a higher resolution than the measurement on U6 and YF in 10/95 [Fig. 23]. Before irradiation U7 was depumped and showed a dark current of a 3 pA. As soon as the irradiation starts current in U7 increases and decreases exponentially afterwards as it was observed on U6 and YF. Before irradiation U7 had the same charge collection distance and contact like U6. At the start of irradiation

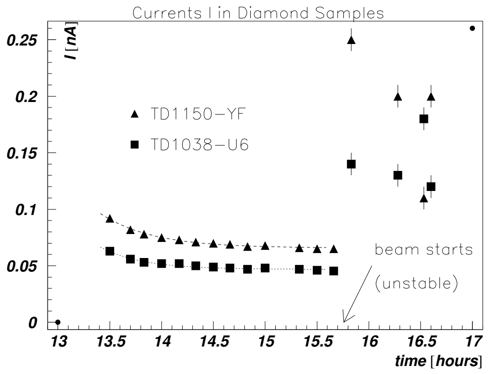

Figure 22: Current in diamond samples, F and U6, before n-irradiation, a few hours before start of the irradiation.

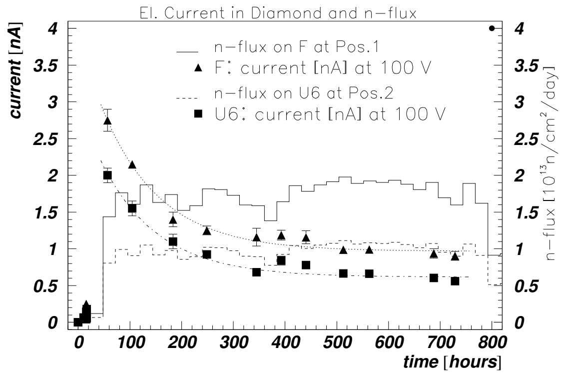

Figure 23: Particle induced current in diamond samples, F and U6, during n-irradiation 10/95. The current in both samples decreases exponentially with the same slope.

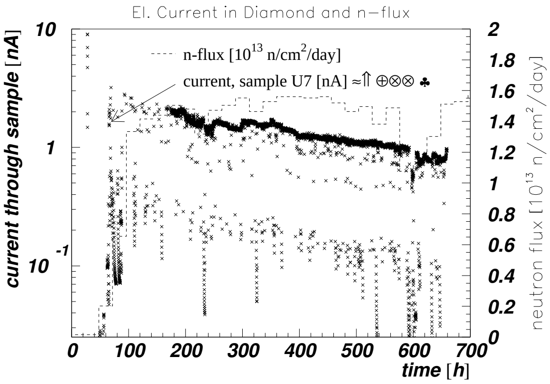

Figure 24: Particle induced current in CVD diamond samples, U7, during n-irradiation 12/95. The current decreases exponentially.

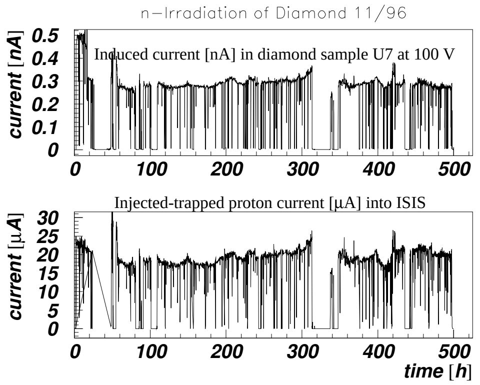

Figure 25: Above, particle induced current in sample U7 during irradiation in 11/96. Below, proton current which is proportional to the n-flux. U7 is being irradiated the second time and the current stays constant.

the current in U7 reaches the same value of about 2 nA as it was measured on U6. Like in the irradiation on U6 one observes a decreasing current at a nearly constant daily flux. The current frequently falls off to its darkcurrent value which is due to spill breaks in the proton accelerator (see below).

The same sample was irradiated a second time in 11/96 and its induced current was measured [Fig. 25]. At the start of the irradiation the particle induced current is at 0.3 nA which is lower than expected from the final value in 12/95. The current in U7 falls off during spill breaks which is confirmed by the measurement of the proton current [Fig. 25, below]. Now it is important to notice that the induced current in U7 does not decrease during irradiation. Its mean current stays constant during irradiation which indicates that the current really saturates and stabilizes after a certain time and fluence. Fig. 26 to 31 show a collection of current during 11/96 irradiation. Currents were measured on samples N1, N2, N3, U6 and Y1 which were all irradiated before and no decreasing current was observed during their second irradiation. Two samples P3 and P4 were irradiated in 11/96 for the first time. Their currents decrease exponentially like in U7, U6 and YF when they were irradiated for the first time.

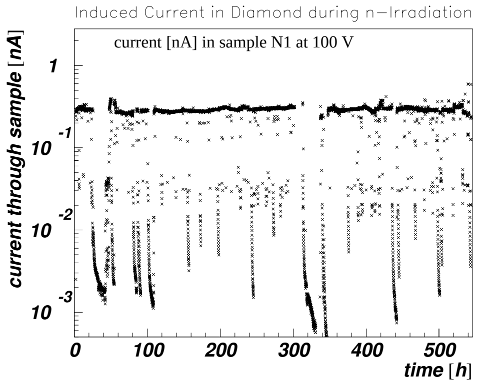

Figure 26: Particle induced current in N1 during neutron irradiation 11/96.

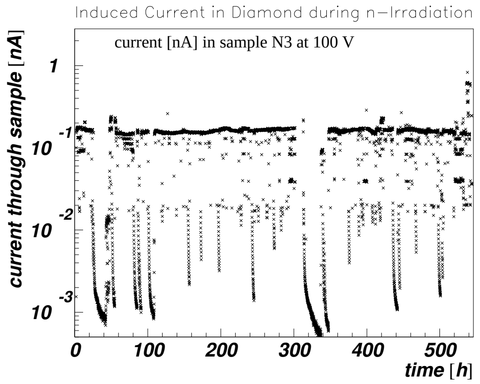

Figure 27: Particle induced current in N3 during neutron irradiation 11/96

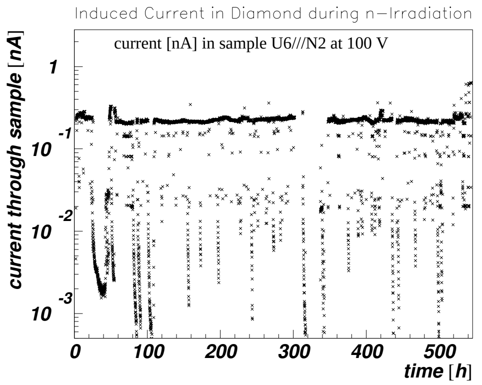

Figure 28: Particle induced current in U6 parallel to N2 during neutron irradiation 11/96

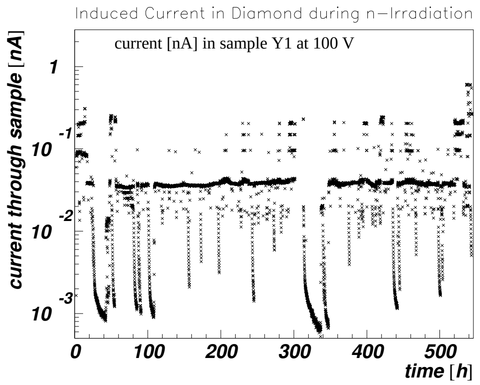

Figure 29: Particle induced current in Y1 during neutron irradiation 11/96

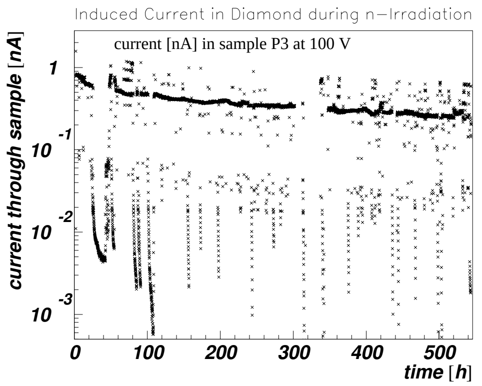

Figure 30: Particle induced current in P3 during neutron irradiation 11/96

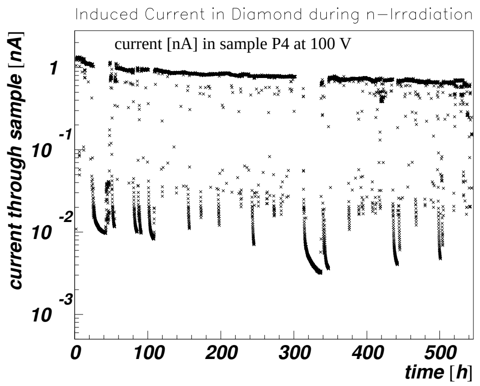

Figure 31: Particle induced current in P4 during neutron irradiation 11/96

4.3 Current during Beam-Off Periodes

The current in U7 decreases as soon as the proton beam is off and no interaction takes place in the graphite block which is shown in Fig. 32. The absolute current 1 hour after the beam was lost decreases in time [Fig. 33]. The current during beam-off periodes is equal to the dark current on U7 which was measured before and after irradiation (see above). At the start of the irradiation the dark current saturates at 100 pA which is the known dark current of the pumped state. At the end of the irradiation the dark current saturates at about 15 pA. This indicates that the sample depumps during irradiaton. Charge collection measurements show that samples are pumped after irradiation which contradicts observations on the current.

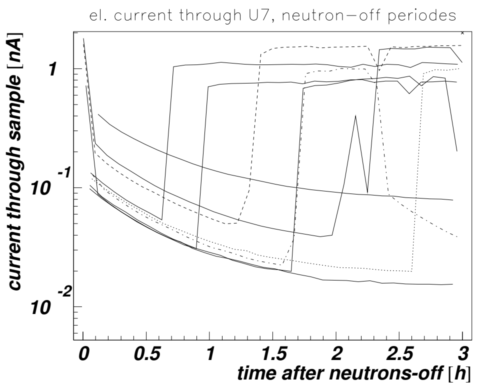

Figure 32: Overlayed current in U7 during beam-off periodes in irradiation 12/95. The current decreases during beam off periodes with the same slope. The absolute current decreases from one beam-off periode to the other.

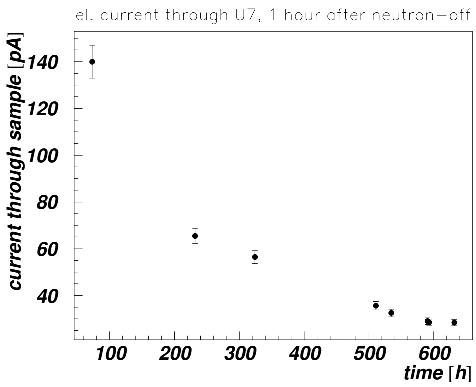

Figure 33: Current in U7 one our after beam was lost. The current decreases in time.

4.4 Induced Current correlates with Neutron Flux and Fluence

The particle induced current in diamond is well correlated with the proton current which is demonstrated for U7 in Fig. 34. Small variations of the proton intensity result in current changes measured in diamond. The diamond sample can be regarded as a neutron flux monitor. Only those samples which were irradiated once before work as a reliable flux monitor. Integration of proton- and induced diamond current in time gives the neutron fluence $F_n(t)$ and the induced charge

$$Q_{\mathrm{pic}}(t) = \int_0^t I_{\mathrm{pic}}(\tau)\,\mathrm{d}\tau \propto F_n(t)\,. \tag{5}$$

Fig. 35 shows the induced charge in diamond and the neutron fluence as a function of time. The neutron fluence was measured by integration of the proton flux on the spallation source. Both graphs show the same slope and plateau as soon as no neutrons are present. Therefore the induced charge is found to be proportional to the neutron fluence. The diamond sample works as a neutron fluence monitor.

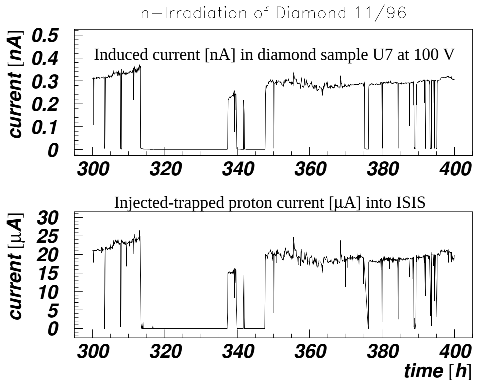

Figure 34: Above, particle induced current in sample U7 in 11/96 for an arbitray time intervall. Below the difference between injected and trapped proton current which is proportional to the n-flux. The current in diamond correlates with the n-flux.

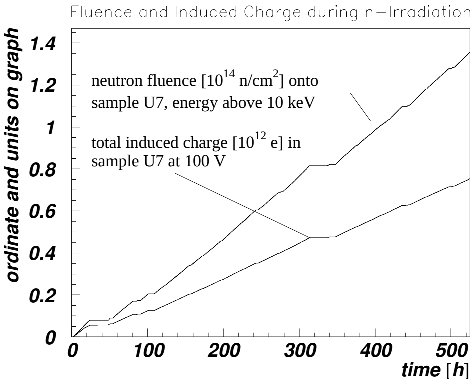

Figure 35: Neutron Fluence and time integrated current in diamond versus time. The neutron fluence was measured by the number of protons which interact in the graphite block.

5 Comparision with Irradiated Silicon Diodes

Irradiation studies of silicon are of special interest since major parts of vertex detectors in experiments at the LHC will be built with silicon detectors. During irradiations of diamonds at ISIS silicon diodes were irradiated as well. They were kept under the same conditions as diamond. Although these conditions are different than they will be in LHC experiments. Experiments at LHC will provide cooling of the silicon detector to -5°C which reduces consequencese of radiation damage. Silicon samples in the n-irradiation were at 19°C and therefore in a hostile environment. Silicon diodes and one strip detector were produced at CSEM [12] with a p-doped implant on a n-substrate. The diodes had a thickness of 350 μm and an implant area of 4×4 mm^2. The strip detector was 350 μm thick with 2 cm long strips and a pitch of 50 μm.

The leakage current of a silicon diode before and after n-irradiation is shown in Fig 36. Before irradiation the current shows the known characteristic of a reversed biased diode. It increases gradually from 0 to 1 nA between 0 and 75 V. The diode is fully depleated at 50 V. Above 80 V the current increases linear to 6 nA at 100 V. After irradiation with 3.2×10^{14} n/cm^2 and a time of 6 months at roomtemperature in darkness the current is higher by a factor 10^2. It increases with voltage linearly from 0 to 1 μA between 0 and 300 V. The silicon sample turned from a diode into an ohmic resistor with a resistance of $R = 330$ MΩ which corresponds to a resitivity of $\rho = 1.5$ GΩcm.

The charge signal measured on this silicon diode before and after irradiation is shown in Fig. 37. Before irradiation a mean number of 35000 e is collected when an electron from the ^{90}Sr source traversed the fully depleated diode which agrees within 10% with the expected value taking the by a *mip* in average generated number of 90 e/μm in silicon. Below 50 V the diode is not fully depleated and only a fractional charge is collected. After irradiation with 3.2×10^{14} n/cm^2 no charge could be detected. Even at higher bias voltage of 200 V no signal is visible.

It is of interest to compare the current of a silicon diode during irradiation with a characteristic current measured in diamond [Fig. 38]. The current in the silicon diode increases non linear in time from a few nA to more than 60 μA. The superimposed current in diamond stays at 300 pA constant in time when neutrons are generated. During beam-off periodes, which are visible in diamond when the current drops to a few pA, a decreasing current in silicon is observed. This effect is known and due to annealing in the silicon lattice. The current measured during irradiation in silicon is not a particle induced current. It is rather a leakage current I_{leak}, since it does not drop like the current

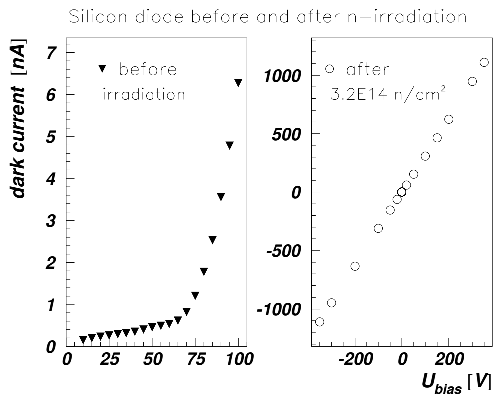

Figure 36: Current versus voltage characteristic in a silicon diode before and after n-irradiation. The diode received a fluence of 3.2×10^{14} n/cm^2.

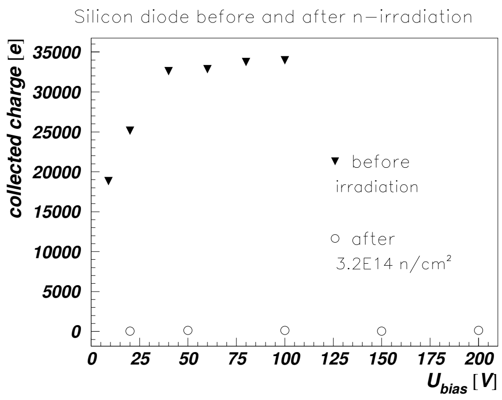

Figure 37: Collected charge in a silicon diode before and after n-irradiation.

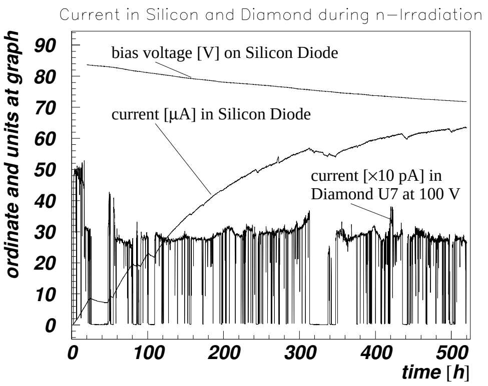

Figure 38: Current and bias voltage in silicon diode S-16 and current in diamond U7 vesus time during neutron irradiation. The diode is biased with a batterie and its voltage decreases linearly due to the high current in the diode, whereas the voltage applied to the diamond stays constant at 100V.

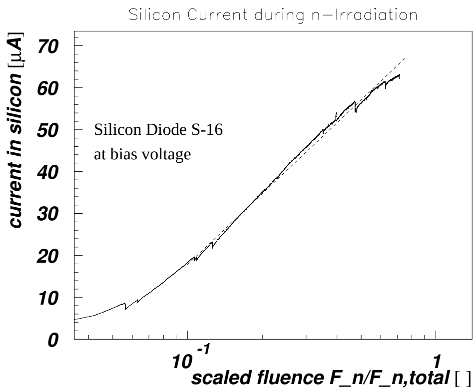

Figure 39: Current in silicon diode S-16 versus integrated current in diamond U7 during neutron irradiation.

in diamond as soon as the beam is off. The leakage current in silicon versus neutron fluence F_n is described by the following empirical expression

$$I_{\mathrm{leak}}(F_n) = I_{\mathrm{leak}}(F_n = 0) + \alpha F_n A D. \tag{6}$$

The value α is the leakage current constant which describes the slope of the leakage current as a funciton of the neutron fluence. The measurement of the leakage current in silicon diodes during irradiation shows indeed a linear increase with neutron fluence up to about 5×10^{13} n/cm^2. The damage constant is in this range measured to $\alpha = 1 \times 10^{-17}$ A/cm in agreement with measurements listed in [13]. At fluences above 1×10^{14} n/cm^2 the leakage current increases logarithmical [Fig.39].

6 Infrared Absorption and Relative Hydrogen Concentration

It was reported that conductivity of diamond depends on the concentration of hydrogen [14, 15]. On one side hydrogenation results in increasing conductivity on the other side annealing

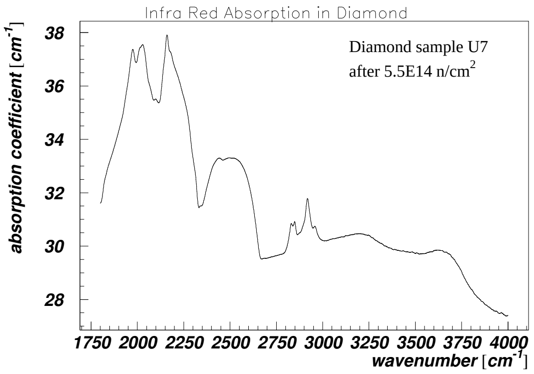

Figure 40: Infrared absorption coefficient of sample U7 after receiving a fluence of 5.5×10^{14} n/cm^2.

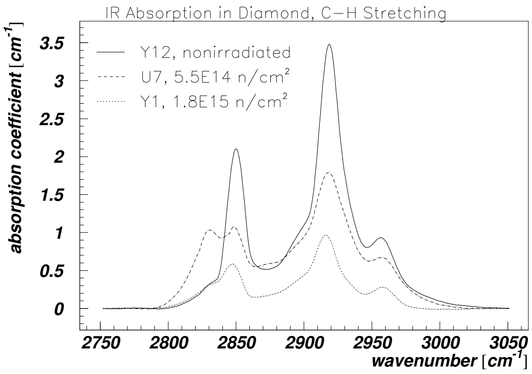

Figure 41: Infrared absorption due to C-H stretching on diamond samples at different n-fluences.

at temperatures up to 400 °C shows a decreasing conductivity. The increase in conductivity is explained by removal of hydrogen from an electrically active to a nonelectrically active site. It is assumed that hydrogen passivates trap levels in the bandgap.

The crossection for interaction of neutrons with a kinetic energy below 10 MeV with hydrogen in diamond is higher than with carbon [Fig. 42]. The change of resistivity in diamond after neutron irradiation motivates to measure the concentration of hydrogen. The concentration of hydrogen in irradiated diamond was measured by infrared absorption. The infrared transmission spectra is sensitive to the number N_{CH} of C-H bonds [16]. The transmission T at a given frequency in a diamond sample of thickness D is given by Beer's law $T = T_0 e^{-\beta D}$ where T_0 is the transmission measured without a sample. The absorption coefficient $\beta = \sigma_{\mathrm{CH}} n_{\mathrm{CH}}$ depends on the concentration $n_{\mathrm{CH}} = \Delta N_{\mathrm{CH}}/\Delta V$ of hydrogen per volume ΔV and on the absorption crossection σ_{CH} of infrared light. The crossection ($\sigma = 2.6 \times 10^{-19}$ cm^2) of C-H bonds with light can be taken from [17] and the conctentration of hydrogyn could be calculated absolutely.

The infrared absorption coefficient on an irradiated diamond sample U7 as a function of the incident wavenumber is shown in Fig. 40. The peaks which are attributed to C-H bonds are visible between 2750 cm^{-1} and 3050 cm^{-1}. The absorption coefficient for this interval measured on several irradiated diamonds is shown relative to its background in Fig. 41. The highest absorption coefficients was meausured on an unirradiated sample. With an increasing neutron fluence the peak maxima decrease which corresponds to an decreasing concentration of hydrogen in the samples.

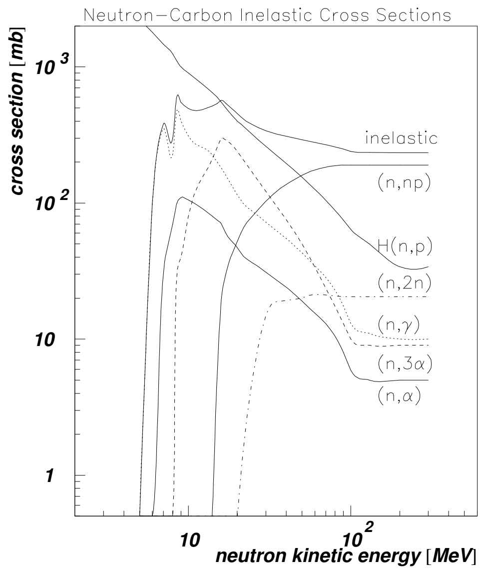

Figure 42: Neutron Carbon inelastic cross sections [18].

7 Conclusion

CVD diamond samples were irradiated with neutrons at the ISIS spallation source. Thermal neutrons up to 2.7×10^{15} n/cm^2 cause no decrease in charge collection distance. The majority of samples were exposed to fast neutron peaking at 1 MeV. Charge collection distance on these samples stays constant up to 5×10^{14} n/cm^2. Above 5×10^{14} n/cm^2 samples behave different. One sample (N3) decreases to 50% at $\approx 8 \times 10^{14}$ n/cm^2, another sample (Y1) decreases only above $\approx 1.3 \times 10^{15}$ n/cm^2 and drops by 35% at $\approx 2 \times 10^{15}$ n/cm^2.

The particle induced current correlates with the neutron flux. The induced current in diamond is likely due to the inelastic nuclear interaction in carbon n(C,α)Be or n(C,3α)n. Charged α's interact electromagentically and generate charge carriers which appear as the particle induced current. During a first irradiation dark currents (pA) and particle induced current (nA) decrease. The currents saturate at higher fluences. We do not believe that the current decrease indicates a decreasing charge collection distance since the current changes occure at lower fluences than changes in charge collection distance. We rather believe that the leakage current decreases due to activation of traps which could be partially refilled by charge carriers. Hydrogen passivates traps and is a prominent component of CVD diamond. The relatively large cross section of neutrons with hydrogen supports the idea of hydrogen removal. In a preliminary study we observe a reduced amount of hydrogen in irradiated samples.

The current response in diamond to neutrons is prompt and relaxes 'immediately' as soon as neutrons vanish with a time constant determined by the setup. It is remarkable that diamond responds to neutrons. The current in silicon during irradiation is a pure leakage current and does not respond to neutrons. The silicon diode is blind to neutrons and only gets damaged. The damage anneals during breaks. The response of diamond to neutrons allows to use diamond as a neutron flux monitor and by summation to measure the neutron fluence.

We conclude that CVD diamond is a radiation hard particle detector substrate up to at least 5×10^{14} n/cm^2 without significant loss in charge collection. Leakage current at roomtemperature is negligible (pA) and does not increase during irradiation up to 2×10^{15} n/cm^2.

8 Acknowledgements

We would like to acknowledge the help of M. Edwards and his colleague during irradiation and dosimetry.

References

[1] J.A.J. Matthews. "Effective Silicon Damage Fluences in the ATLAS Inner Detector Extrapolated from CDF". Technical note, University of New Mexico, 10 1996. ATLAS/INDET-NO-145.

[2] ATLAS, Technical Proposal. LHCC/94-43/P2, 1994.

[3] M.H. Nazaré *et al.* (RD42-Collaboration). "Development of Diamond Tracking Detectors for High Luminosity Experiments at the LHC". RD42-Proposal, CERN, (May. 1994). DRDC 94-21/P56.

[4] RD42-Collaboration. First Measurements with a Diamond Microstrip Detector. *Nuclear Instruments and Methods*, A(354):318–327, 1994.

[5] W. Adam *et al.* (RD42-Collaboration). "Development of Diamond Tracking Detectors for High Luminosity Experiments at the LHC". Status Report/RD42, CERN, (Jan. 1997). LHCC 97-3.

[6] W. Dulinski. "Electron Irradiation of CVD Diamond". RD42 Collaboration Meeting Notes, (Jun. 1995).

[7] D. Meier *et al.* (RD42-Collaboration). "Proton Irradiation Study of CVD Diamond Detector Samples for LHC", (1997). RD42 Internal Note 10.

[8] St. Gobain/Norton Diamond Film, Goddard Road, Northboro, MA 01532, USA.

[9] DeBeers Industrial Diamond Division Ltd., Charters, Sunninghill, Ascot, Berkshire, SL5 9PX England.

[10] M. Edwards and D.R. Perry. "The Radiation Rardness Test Facility". *RAL Report*, RAL-90-065:p.21, (1990).

[11] S. Zhao. *"Characterization of the Electrical Properties of Polycrystalline Diamond Films"*. PhD thesis, Ph.D. Dissertation, Ohio State University, (1994).

[12] Centre Suisse d'Electronique et de Microtechnique SA, Rue Jaquet-Droz 1, P.O. Box 41, CH-2007 Neuchtel, Switzerland.

[13] E.Borchi and M.Bruzzi. "Radiation Damage in Silicon Detectors". *La Rivista del Nuovo Cimiento*, 17(11), (1994).

[14] M.I. Landstrass and K.V. Ravi. "Hydrogen Passivation of electrically active Defects in Diamond". *Appl. Phys. Letters*, 55:1391–1393, (1989).

[15] Sacharia Albin and Linwood Watkins. "Current-Voltage Characteristics of Thin Film and Bulk Diamond Treated in Hydrogen Plasma". *IEEE Electron Device Letters*, 11(4):159–161, (1990).

[16] K.A. Snail. "Growth, Processing and Properties of CVD Diamond for Optical Applications". *Optical Materials*, 1(4):235–258, (1992).

[17] find out! "has to be checked!". *Diamond Optics V*, 1759:204–208, (1992).

[18] R.A.Cecil *et al.* "Improved Predictions of Neutron Detection Efficiency for Hydrocarbon Scintillators from 1 MeV to about 300 MeV". *NIM*, 161:439–447, (1979).